Ablation of gold into water

N A Inogamov[1,2], V A Khokhlov[1], V V Zhakhovsky[2,1], K V Khishchenko[3] and S I Anisimov[1]

[1] Landau Institute for Theoretical Physics of the Russian Academy of Scienses, Akademika Semenova 1a, Chernogolovka, Moscow Region 142432, Russia
[2] Dukhov Research Institute of Automatics (VNIIA), Sushchevskaya 22, Moscow 127055, Russia
[3] Joint Institute for High Temperatures of the Russian Academy of Sciences, Izhorskaya 13 Bldg 2, Moscow 125412, Russia

E-mail: nailinogamov@gmail.com

23 February 2017

Abstract. Using the contacting pair gold-water we consider problems connected with description of femtosecond laser pulse action onto metallic target immersed into transparent liquid. Results of two-temperature one-dimensional hydrodynamic simulations are presented. Water strongly decelerates the expanding contact boundary between metal and liquid. In the non-inertial frame fasten to the contact the deceleration transfers to gravity field according to the Einstein's principle of the equivalence between gravitational and inertial mass. Thus dense molten gold appears above small density liquid (water). Such quasi-hydrostatic equilibrium is unstable against Rayleigh-Taylor (RT) instability (RTI). Results of large scale molecular dynamics (MD) simulations also are given. They confirm that the RT amplification of the contact surface disturbances takes place. MD pictures reveal the process of formation of alternating water bubbles penetrating into liquid gold and jets of gold falling into water. Decay of the jets into droplets is one of the possible mechanisms of creation of nanoparticles.

PACS numbers: 52.38.Mf, 79.20.Ds, 79.20.Eb

Keywords: laser ablation in liquid, molecular dynamics, Rayleigh-Taylor instability

1. Introduction

Ultrashort pulse laser ablation is used for production of nanoparticles [1–6]. This way of production has clear distinctions from the chemical synthesis of nanoparticles. The main advantage of the chemical synthesis is its low price. But chemical process include many intermediate steps, products may be limited in size and size distribution and have traces of undesirable contaminations. Laser ablation is qualitatively different, the corresponding procedure is simple and straightforward, the colloidal products are chemically clear. Also using lasers we can vary targets from bulk to films or laminates, change their chemical compositions, and/or we can change illumination conditions, thus obtaining different in size nanoparticles of wide range of materials.

In spite of importance of the fundamental problem of laser-matter interaction in surrounding media and laser generation of nanoparticles, it remains not well understood. Recently interesting theoretical papers appeared dealing with this problem [7–12]. From general point of view there are two mechanisms of particle formation [7, 8, 12]. The first is usually considered. It is the condensation mechanism. The second is connected with hydrodynamic instability around the metal-water contact. Their relative importance depends on absorbed energy $F_{\rm abs}$. The first mechanism dominates at very high values of $F_{\rm abs}$. In the paper below we concentrate on the second mechanism at $F_{\rm abs} = 400$ mJ/cm^2.

The difficult case of a bulk target in bulk water is considered. This case is more complicated compared to the case of a thin film with thickness of the order of 10 nm. We will see below that there are shock in water, shock compressed layer of water, the gold-water contact jump, "atmosphere" made of gold, two-phase vapor-liquid foam, and remnant of gold target. Atmosphere presses on water, while water decelerates the atmosphere. Mass of atmosphere increases because it decelerates while internal foamy vapor-liquid mixture expands inertially (no deceleration) thus having larger velocities and thus sprinkling onto atmosphere. This process delays deceleration of atmosphere, prolongs dynamic interaction through gold-water contact, and makes simulation significantly longer in time and spatially more extended relative to the case of a thin film.

2. Hydrodynamic equations and physical model

We consider action of an ultrashort pulse onto plane surface of metal immersed in transparent liquid. Light crosses liquid and is absorbed in a skin-layer of metal. We work below the threshold for optical breakdown of liquid. Our absorbed fluence are rather moderate 0.4 J/cm^2 and pulse is short—its duration is $\tau_L = 0.1$ ps. We consider the practically important case of bulk gold illuminated through a thick layer of water. Threshold for thermomechanical ablation of gold in vacuum is $F_{\rm abs}|_{\rm abl}|_{\rm vac} \approx 0.1$ J/cm^2 [13–15].

We analyze situation using two-temperature (2T) one-dimensional (1D) Lagrangian hydrodynamic code (2T-HD). Corresponding equations are

$$\rho(x^0,t)\frac{\partial x(x^0,t)}{\partial x^0} = \rho^0, \tag{1}$$

$$\rho^0\frac{\partial u}{\partial t} = -\frac{\partial P(x^0,t)}{\partial x^0}, \tag{2}$$

$$\frac{\partial x(x^0,t)}{\partial t} = u(x^0,t), \tag{3}$$

$$\rho^0\,\frac{\partial(E_e/\rho)}{\partial t} = -\frac{\partial q}{\partial x^0} - \dot{E}_{\rm ei} + \frac{\rho^0}{\rho}\,Q - P_e\frac{\partial u}{\partial x^0}, \tag{4}$$

$$\dot{E}_{\rm ei} = \frac{\rho^0}{\rho}\alpha\cdot(T_e - T_i), \qquad q = -\frac{\rho\kappa}{\rho^0}\,\frac{\partial T_e}{\partial x^0}, \tag{5}$$

$$\rho^0\,\frac{\partial(E_i/\rho)}{\partial t} = \dot{E}_{\rm ei} - P_i\frac{\partial u}{\partial x^0}, \tag{6}$$

$$Q = \frac{F_{\rm abs}}{\sqrt{\pi}\,\tau_L\,\delta}\exp\left(-\frac{t^2}{\tau_L^2}\right)\exp\left(-\frac{x}{\delta}\right)\theta(x). \tag{7}$$

Above we write conservation of mass (1); ρ^0 is initial density. Trajectory of material particle with Lagrangian coordinate x^0 is $x(x^0,t)$. Lagrangian coordinate is defined as $x(x^0, t=-\infty) = x^0$. equation (2) presents momentum conservation; here $u(x^0,t)$ is velocity of Lagrangian particle. Kinematic condition is (3).

Energy conservation is written separately for electron and ion subsystems as it was proposed in the pioneering paper [16]. Energy balance in electron subsystem is given by equation (4). Energy exchange power between electron and ion subsystems per unit of volume and electron thermal conduction flux are given by expressions (5). Equation (6) describes ion energy balance.

Laser source power per unit of volume connected with absorption of light is (7). In this equation the

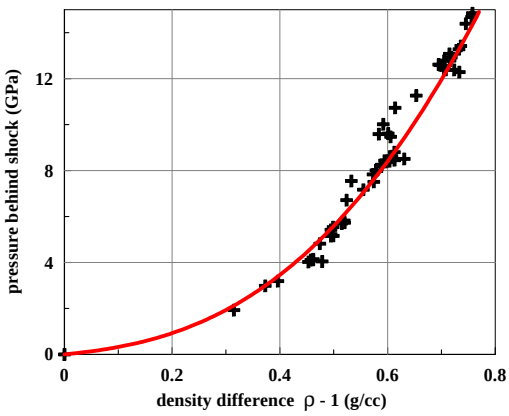

Figure 1. Hugoniot adiabatic curve of water in the range of moderate compressions: markers present experimental data from [22], the curve corresponds to approximation (8) valid in the wide pressure range, see figure 2.

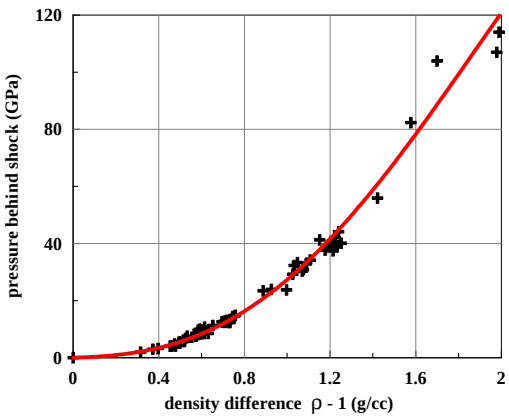

Figure 2. Shock wave adiabatic curve from [22] (markers). The curve shows dependence (8).

thickness of a skin layer is δ, τ_L is duration of pulse. Expression (7) with function $\theta(x) = 1, x > 0$, $\theta(x) = 0, x < 0$ is valid for ultrashort laser pulse of moderate intensity when we can neglect the shift of a contact boundary during the pulse. At the initial instant the contact is placed in the point $x = 0$. Absorbing metal initially is located at the right side $x > 0$.

To solve the system presented above we need data which in continuous manner describe matter in its states from 2T to 1T (one-temperature) stages. We use modern data about equation of state, electron heat conduction κ and electron-ion coupling parameter α. equation of state for gold follows from approximate description as a sum of electron and ion free energies [17–19]. The ionic part is taken from the wide range equation of state [20–22].

In the 2T-HD runs presented below, the water obeys approximation

$$p = 2.25x + 7.07x^2 + 25.08x^3 - 7.04x^4, \quad x = \rho - 1, \quad (8)$$

here pressure p is in GPa, density ρ is in g/cc. The approximation (8) corresponds to shock wave data collected in [22]. The approximation (8) gives correct value of sound speed 1.5 km/s at weak compressions and remains valid up to the end of the measured data at pressures ~ 100 GPa. Comparison of approximation (8) with experimental values is shown in figures 1 and 2. It is significant that the unload adiabatic curve returns back approximately along the same dependence (8).

In the 2T-HD code at the level given below, we neglect very small thermal conductivity of water. It will be included in future work. For molecular dynamics (MD) simulations we develop effective interatomic potential for water, which describes molecules of water as points. In MD the thermal conductivity of water is present. It is connected with thermal molecular motion.

Important role belongs to thermal conductivity of gold. It is especially large at the 2T stage. In 2T-HD we employ conductivity model developed in papers [23–27]. Equally important is knowledge about electron-ion coupling parameter α. We use the approach developed in papers [23, 26–28]. In 2T-HD the approximation

$$\alpha(\rho, T_e) = (\rho/\rho_0)^{5/3} \times \left(0.2 + \frac{4.3}{K_\alpha} \frac{T_{\rm eV}^{3.6}}{1 + T_{\rm eV}^{3.5} + 0.9 T_{\rm eV}^{4.1}}\right) 10^{17}\,[{\rm W/K/m^3}] \quad (9)$$

has been applied. In (9) electron temperature $T_{\rm eV}$ is in [eV]. The parameter K_α defines value of coupling in gold at the elevated temperatures T_e.

At low temperatures T_e the expression (9) begins from the experimentally measured value 0.2×10^{17} W/K/m^3 [29]. Influence of variation of K_α in the range from 1 to 6 has been considered in [28]. Values of K_α near 1 approximately corresponds to the dependence $\alpha(\rho_0, T_e)$ given in paper [30]. If $K_\alpha \approx 1$ then function (9) rises ten times when temperature T_e increases above the values $T_e \sim (5 - 10)$ kK. If $K_\alpha \approx 4 \div 6$ then the rise of $\alpha(\rho_0, T_e)$ with T_e above 10 kK is much weaker- coupling increases 1.5-3 times relative to value of α at room temperatures. Experimental data collected in paper [31] support opinion about weak rise of coupling α with temperature T_e. At $K_\alpha \approx 1$ the electron-ion temperature relaxation in gold is faster than in the case with $K_\alpha \approx 4 \div 6$. Below we consider the case with strong coupling $K_\alpha = 1.15$.

3. Two-temperature relaxation

The 2T stage lasting the first few picoseconds after the subpicosecond optical heating of gold is the same as in the case with vacuum if absorbed fluences are the same. Thus the 2T melting is also the same. But sometimes authors say opposite. 2T-HD simulation of this stage is shown in figures 3 and 4. The convergence of T_e and T_i profiles is clear from figure 3. The convergence is

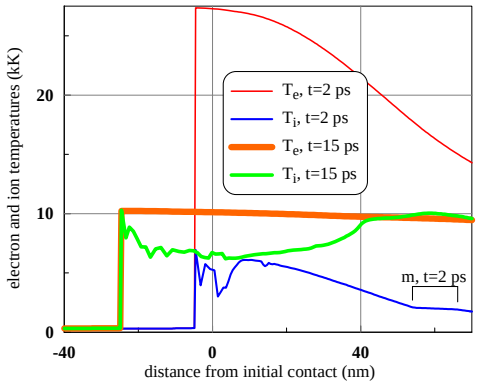

Figure 3. 2T relaxation and expansion of gold at the early stage after laser impact; $F_{\rm abs} = 400$ mJ/cm^2, duration $\tau_L = 0.1$ ps. Time is reckoned from the maximum of the heating pulse, see (7). The note "m" marks position and thickness of the melting two-phase (solid-liquid) zone at 2 ps. In this zone the gold gradually transits from solid to liquid state. Analysis of comparison between supersonic meltings in two-temperature hydrodynamics and in molecular dynamics is presented in [32, 33].

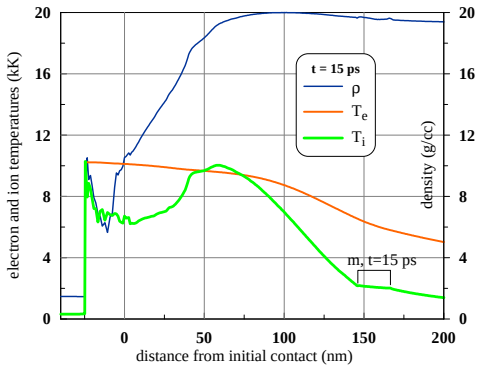

Figure 4. Electron T_e and ion T_i temperature profile at the nominally 1T stage. Nevertheless there are appreciable differences between local values of temperatures, see explanations in the text; Au-water, $F_{\rm abs} = 400$ mJ/cm^2, $\tau_L = 0.1$ ps.

accompanied with fast penetration of absorbed energy into depth of a bulk gold sample due to high electron heat conduction.

At the temporal range around $\sim$ 10 ps the propagation of the melting zone "m" is still supersonic: the zone "m" shifts from 60 to 160 nm during the temporal interval from 2 to 15 ps, see figures 3 and 4. While the head characteristics of the rarefaction wave at 15 ps achieves only distance 60 nm from initial position of the contact. Speed of sound increases relative to its cold value ≈ 3 km/s thanks to additional elasticity linked to electron pressure and heating of lattice. But melting brings down this speed.

Melting zone "m" in figures 3 and 4 consists of a mixture of solid and liquid phases. The melting process in 2T-HD and in MD is compared in [32, 33]. The comparisons demonstrate that description of the temperature profile, volume ratio of solid and liquid phases are similar in both approaches. Melting proceeds at elevated pressures. Therefore temperatures T_i in the melting zone are higher than temperature in the triple point [33].

Sharp decrease of temperatures and densities (contact jump) in figures 3 and 4 takes place at the contact between hot gold and cold water.

Large difference between T_e and T_i (tens of kK) existed during a few first picoseconds (see figure 3) disappears at the stage 5-10 ps. At this stage the electron internal energy transferred into ions is few times larger than energy remaining in electrons. Nevertheless even at the stage 15-20 ps there is significant difference between temperatures T_e and T_i, see figure 4. There are two regions and two sources of this difference. They locate: one to the left side of the total pressure p and temperature T_i instant maximum in figure 4 and another one around the melting zone "m". The first region is the region occupied at this temporal stage by rarefaction wave, here ions cool because of strong expansion in the high amplitude rarefaction. In the second region the difference between the temperatures T_e and T_i is caused by energy expenses going to melting of solid gold (heat of fusion). Thus maximum of temperature T_i appears. Electron temperature T_e profile is more smeared due to high electron conductivity.

In the rarefaction wave in figure 4 the density of gold drops down close to the critical value of density which is 5.3 g/cc according to the wide-range equation of state [20–22] used in simulations. Expansion is energetically supported by decrease of internal energy of ionic subsystem which cools ions. Of course, expansion also cools electrons, but as was said large conduction smooths out the profile of T_e.

The stage shown in figures 3 and 4 finishes with formation of heat affected zone (HAZ). Its thickness is $d_T \sim 150$ nm for gold. Formation of the HAZ proceeds fast (supersonically) thanks to high electron conduction at the 2T stage. This process is independent on presence or absence of water. We can speak about expansive expenses of internal ion energy and cooling of ions inside the rarefaction wave in the HAZ at the stage lasting up to $t < t_s \approx 50$ ps; here $t_s = d_T/c_s$ is acoustic time scale. Later in time the rarefaction leaves the heat affected zone. Temperatures T_e and T_i are small outside the zone d_T. The HAZ is created faster than the rarefaction leaves the HAZ: first conduction produces HAZ, and after that, at acoustic time scale, rarefaction leaves the HAZ.

4. Atmosphere, nucleation, and foaming

It is well-known that fast increase of pressure in the HAZ induces expansion of gold. Matter

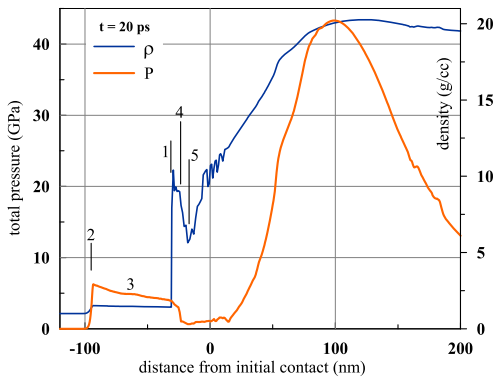

Figure 5. The structure of expanding gold plume in the case when water is present, $t = 20$ ps, $F_{\rm abs} = 400$ mJ/cm^2. The decreases of density and pressure from left to right between the left boundary 1 and the right boundary 5 of atmosphere is caused by effective gravity g acting on gold in the frame comoving with contact 1. Gold falls into "trap" of atmosphere through the boundary 5 separating the decelerating atmosphere and the freely expanding plume. The interval occupied by atmosphere is numerated by 4. There is decrease of density in the rarefaction wave filling the left side relative to the maximum of pressure where the head of rarefaction locates at this snapshot. Oscillations of density at the left edge of rarefaction correspond to the nucleation process.

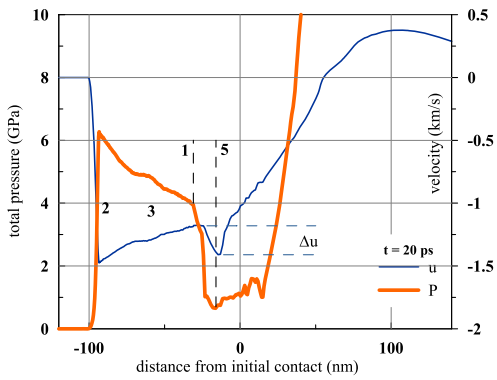

Figure 6. The enlarged view of the previous figure 5. This view shows the near contact structure of the coexisting layers. Expansion velocity has a jump Δu at the upper boundary 5—shock 5 sharply decelerates expansion. We call it the "upper" boundary relative to the vector g of "free fall acceleration" existing in the non-inertial frame attached to the decelerating contact 1. Weight of heavy gold in atmosphere together with pressure jump at the shock 5 define the pressure difference between the planes 1 and 5.

expands in rarefaction wave running into bulk. The rarefaction head and expanding matter move in opposite directions. In linear acoustic approximation, hydrodynamic velocity of expansion (velocity of contact boundary CB) into vacuum is equal to

$$u_{\rm CB} = p/z = c_s\,(p/B) = 1.7\,p_1\,[\text{km/s}], \qquad (10)$$

where $p = G\,E$ is pressure created by heating, p_1 is pressure in Megabars, $z = \rho\,c_s$ is acoustic impedance, $B = 180$ GPa is bulk modulus of gold, E is internal energy per unit of volume; Gruneisen parameter G changes during 2T stage from electron $G_e \approx 1$ to ion $G_i \approx 3$ value. In our case expansion proceeds into water. Gold has 30 times higher impedance than water. Therefore the estimate $u_{\rm CB} \approx 1.7\,p_1$ km/s of contact velocity approximately remains. Thus quantitatively presence of water weakly changes the maximum value of contact velocity. Here we speak about the contact between two homogeneous semispaces: one is cold water initially under $p = 0$, while the other is hot high-pressure gold.

But the gold semispace cannot be regarded as homogeneous. There is the HAZ with finite thickness d_T. At the early stage the high-pressure region is limited to the HAZ. Namely as result of finite thickness d_T, the expansion caused by decay of pressurized gold semispace into vacuum gradually changes to over-expansion: negative pressures appear at the depth of the order of d_T. Consequently, gradient $(-\nabla p)$ develops in this case in gold near the contact with vacuum. This gradient decelerates the contact. Of course, this is possible only in condensed matter because it has ability to resists to stretching (if matter is gas then $p < 0$ isn't possible).

Spallation phenomena and thermomechanical ablation follow from negative internal pressures and strength of matter. There is the mentioned above ablation threshold $F_{\rm abs}|_{\rm abl}|_{\rm vac} \approx 100$ mJ/cm^2 for gold in case of expansion to vacuum. Spallation or ablation means that a layer of finite mass flies away from a target. But in case of infinitely thick layer of water (contacting with target) the flight away becomes impossible for one-dimensional (1D) spalled layer. Indeed, any distant finite pressure in water will finally return back the spalled layer.

It is necessary to break off the continuous contact boundary to bypass this limitation. Gold-water mixing is the key to tear away pieces of gold from the initially continuous bulk gold target. To mix gold with water significant excess above the vacuum threshold $F_{\rm abs}|_{\rm abl}|_{\rm vac} \approx 100$ mJ/cm^2 should be applied. The value at least 3-4 times higher than $F_{\rm abs}|_{\rm abl}|_{\rm vac}$ is required. Therefore we present here results for $F_{\rm abs} = 400$ mJ/cm^2 absorbed during an ultrashort pulse.

Let $\Delta u_{\rm CB}$ is decrease of velocity $u_{\rm CB}$ (10) due to material resistance to stretching. Below threshold $F_{\rm abs}|_{\rm abl}|_{\rm vac}$ the decrease $\Delta u_{\rm CB}$ totally compensates velocity $u_{\rm CB}$ (10). Stopping of contact continues during the temporal interval of the order of acoustic time scale t_s. Above threshold the compensation is only partial—a spallation plate flies away into vacuum with asymptotic velocity $u_{\rm CB} - \Delta u_{\rm CB}$. With increase of the ratio $F/F_{\rm abs}|_{\rm abl}|_{\rm vac}$ the value $u_{\rm CB}$ increases while the value $\Delta u_{\rm CB}$ decreases. The decrease of $\Delta u_{\rm CB}$ is connected with heating of nucleation zone

and increase of temperature their, because heating decreases material strength. Increase of this ratio also decreases thickness of the spallation plate $d_{\rm sp}$. There is so called "evaporation" threshold $F_{\rm evap}$ above which the spallation plate disappears: $d_{\rm sp} = 0$.

Absorbed fluence $F_{\rm abs} = 400$ mJ/cm^2 is of the order of evaporation threshold $F_{\rm evap}$ for expansion into vacuum. Above the threshold $F_{\rm evap}$ we have
(i) The decrease of contact velocity $\Delta u_{\rm CB}$ disappears.
(ii) Spallation plate is absent: $d_{\rm sp} = 0$.
(iii) Density profile (at the stage significantly after nucleation) becomes monotonically decreasing in direction to vacuum.

While in the range

$$F_{\rm abs}|_{\rm abl}|_{\rm vac} < F_{\rm abs} < F_{\rm evap}$$

the ρ-profile is nonmonotonic. It has depletion of average mass density (averaged over local volume) between density in bulk and density of spallation plate.
(iv) Molten layer is thick. Liquid gold cavitates at large depth. Due to stretching of liquid a spacious plume forms.

Presence of water causes important qualitative transformation of the near-contact layers. Again density depletion appears; although we are above $F_{\rm evap}$ for expansion in vacuum. But now the rise of density near the contact is caused not by presence of spallation plate, but by forming of the atmospheric layer 4 shown in figure 5. The principal differences with the case of vacuum are located on the both sides of the contact 1 in figures 5 and 6. Inertia of water displaced by expanding gold dynamically affects the left edge of a gold plume. There are the shock 2 in water and the shock compressed water layer 3 shown in figures 5, 6. Inertial resistance of water to displacement causes appearance of the water affected layer of gold (the atmosphere 4) which comoves hydrostatically with the contact 1.

Water is much "weaker" than gold. As was said the impedance ratio is approximately 30 (Au versus water) while density ratio is near 20. Therefore deceleration by water lasts long period of time; long in comparison with acoustic scale $t_s \sim 50$ps. While at the acoustic time scale the atmosphere is geometrically thin relative to the plume. Outside the atmosphere the plume doesn't know about water. The upper boundary 5 (see figures 5, 6) of the atmosphere separates the parts of gold target knowing and don't knowing about water. Thus the boundary 5 is a weak shock.

Speed of sound c_s at the edge of the plume is low. Here gold expands down (in the ρ, T plane) to the near critical region: densities decrease to 5-6 g/cm^3 (figures 5, 6), pressures fall down to ~ 1 GPa, temperatures are ≈ 6 kK, see figure 4. This is unloaded (at the shown snapshots) layer located at the right side relative to

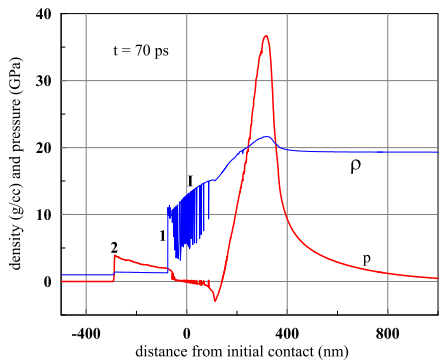

Figure 7. Gold-water interacting region shown entirely from shock 2 in water to compression wave propagating to the right in bulk gold. The contact and nucleation layer are in between these two edges. Density profile sharply fluctuates due to nucleations. Pressure in the nucleation layer drops to low values relative to values in the left and right compression waves.

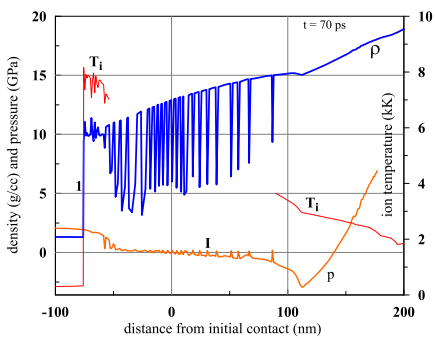

Figure 8. Enlarged view onto the contact and foam. The view is taken from previous figure 7. Profiles of density, pressure, and temperature are presented.

the shock 5 in figures 5 and 6. This layer is unloaded thanks to expansion and fragmentation of the plume. Matter in this layer moves supersonically relative to its local small speed of sound.

Gold is compressed back by its weight in atmosphere 4 when it transfers through the shock 5. Pressure and temperature rise as a result of compression and matter leaves the region of the near-critical states. Matter shifts to the right and up from a critical point at the ρ, T phase plane. As was said above, water is "weak" versus gold, therefore at the early stages ($t \sim t_s$) the decrease $\Delta u \approx 0.25$ km/s of expansion velocity of gold (when it passes the shock 5) is small relative to expansion velocity ≈ -1.5 km/s taken in laboratory reference system- presence of water weakly influences expansion velocity. Velocity profile in this frame system and deceleration Δu in a weak shock 5 are shown in figure 6.

The situations similar to the raking of the edge of a supersonically expanding gold plume by resisting water exist in physics of explosions and astrophysics, see review of these situations in [34]. The same

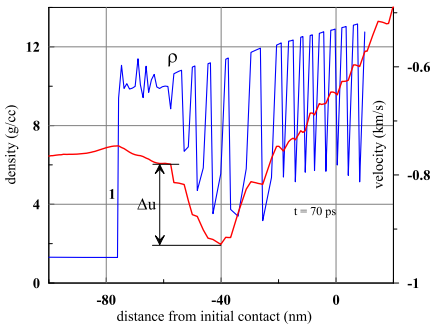

Figure 9. (i) The cut off part of foam (the part to the left side from point I in figures 7 and 8), (ii) atmosphere, and (iii) contact 1 with water. Enlarged view of figure 8 is shown. The point $x = 0$ is the initial position of the contact.

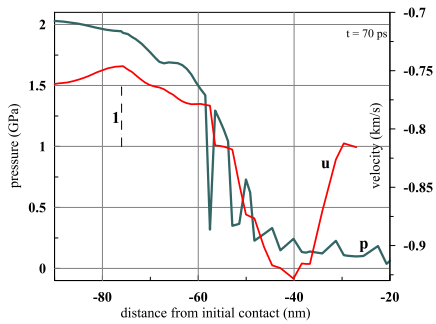

Figure 10. Deceleration of freely expanding foamy mass at the upper bound of atmosphere increases pressure from low values in foam (thousands of bar) to values above critical pressure $p_{\rm crit} \approx 0.53$ GPa=5300 bar for gold; critical parameters are $T_{\rm crit} = 7.8$ kK, $\rho_{\rm crit} = 5.3$ g/cm^3 according to [20–22]. Cavities in foam collapse and foam compresses as a result of impact of foam on atmosphere. Thus a near-critical mixture departs from critical point to higher pressures arriving to the atmosphere. The vertical straight 1 marks instant position of contact.

structure with two shocks around a contact forms when dense detonation products expand into gas. The products rake the gas thus forming two shock and two gravity compressed shells. In astrophysics such structure appears after supernova explosion. The shells may be thin relative to their radius. In the case of high explosives the shell from products is thin because the products are multiatom molecules with adiabatic exponent close to 1. Also the 3D expansion significantly decreases thickness. In astrophysics the radiative loses do the shells thin.

Let's mention once more that deceleration of contact by water and the raking structures around the contact appear because there is a heat affected zone of finite thickness d_T created at the two-temperature stage, see previous Section; in gold $d_T \approx 150$ nm; if $d_T = \infty$ then contact will move with constant velocity (10). Due to continuous raking, the mass of atmosphere gradually increases in time, while a shock in water monotonically decreases its amplitude, transfers in acoustic wave, and travels out to large distances from contact.

5. Middle stage: rupture of foam

In the case $F_{\rm abs} = 400$ mJ/cm^2, $\tau_L = 0.1$ ps considered here, absorbed fluence approximately 4 times overcomes nucleation threshold. Therefore nucleation isn't a once-only event, it proceeds for a long time of the order of the acoustic time scale t_s. There are multiple nucleations following one after another, deeper and deeper into the bulk gold. Finally the nucleated layer has thickness $\sim d_T$. The first nucleations start near the atmosphere (see figure 5 and 6) inside high temperature gold where mechanical resistance to nucleation (strength of material) is very low. Temperatures in the nucleation points decrease as a chain of consecutive nucleations propagates deeper into gold.

A whole picture at the stage when nucleation finishes is presented in figure 7. The left and right edges of a layer in motion are shown. There is a shock 2 in water ahead the compressed water layer between the shock 2 and contact 1 at the left side and powerful compression wave in gold going to the right. For us, analyzing possible water-gold mixing, the intermediate elements of the layered structure are significant. They are the contact and the layer I with multiple cavities. Enlarged pictures of flow near a contact are shown in figures 8-10.

Later in time the nucleated layer expands and gradually transforms into foam like vapor-liquid mixture. Ruptures in this two-phase mixture starts from its left edge and proceeds with time from left to right. The foam after rupture transfers into droplet-vapor mixture. There is a Lagrangian particles of gold in the point I in figures 7 and 8. These particles separate droplets which finally join atmosphere and droplets together with remnants of foam which finally remain at the target and form bottom of the crater at the target surface.

Pressure drops to small values in the foamy gold layer, see figures 7 and 8. Thus dynamically only accretion of liquid fragments from foam is significant for motion of atmosphere. As was said in previous paragraph, the part of the foam located at the left side relative to the point I will gradually accretes onto atmosphere. The part of foam at the right side from the point I cannot influence dynamics of atmosphere because it returns to the rest of the target forming nanostructured bottom of a crater; this structures are observed in experiments, see figure 8 in [35]; they are similar to chaotic nanostructures in case of vacuum [36]. Therefore to simplify our hydrodynamic simulation, we omit (after the instant $t = 70$ ps shown

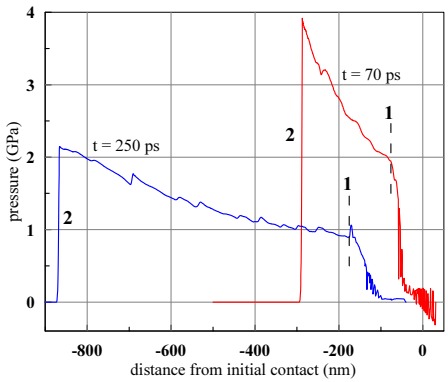

Figure 11. Deceleration of the both trajectories: the shock 2 in water and contact 1. Deceleration of the contact proceeds faster, compare distances passed by the shock and by the contact during 0-70 ps temporal interval and 70-250 ps interval; initially contact was in the point $x = 0$.

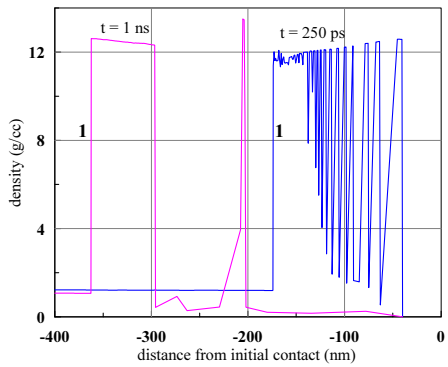

Figure 12. All foam flying to the left side accumulates inside atmosphere during the temporal interval shown here. Thus the reserve stock of mass in two-phase mixture is exhausted. Stopping of momentum supply from accreting foam causes intensification of deceleration of contact. This will be shown below when we will consider a trajectory of contact.

in figures 7-10) the right part of foam together with the continuous rest of a gold target and compression wave moving in it. Instead, we put motionless wall in the point I to prevent gold vapor from expansion to the right side thus keeping vapor inside the cavity between the atmosphere and the rest of a target. The cut off part of foam is shown in figure 9.

Velocity and density instant profiles in vicinity of the contact are shown in figure 9. We see accretion of foamy masses onto atmosphere; accretion is similar to rain when liquid droplets fall down and join to the ground. In figure 9 the upper shock 5 limiting the atmosphere from above (see figures 5, 6) is smeared due to fragmentation of falling masses. Decrease of expansion velocity Δu in figures 9 and 10 marks off the shock 5. Deceleration of expansion velocity $\Delta u(t = 70\,\mathrm{ps})$ is equal to 150 m/s, while velocity of the contact is $u_{\mathrm{CB}}(t = 70\,\mathrm{ps}) = 770$ m/s; compare with figure 6 for $t = 20$ ps where these values were 250 m/s and 1200 m/s, respectively. Atmosphere "sits" on a contact transferring momentum arriving from fast foam to the contact. Foam moves from right to left faster than the contact, see figures 9 and 10.

6. Final stages

Process of deceleration at the subnanosecond time scale is presented in figure 11. Shock 2 in water decreases its amplitude: pressure behind shock and velocity drop down; post shock velocity decreases from 3.6 to 3 km/s. At the early stages deceleration of shock is caused by a continuous slowdown of piston (contact with gold). Later in time the shock transforms into triangular like shape and decelerates due to non-linear expansion of length of the triangular, or it is equally right to say that the shock becomes weaker because of action of a rarefaction wave "attached" to its front. Contact velocity goes down from 750 to 410 m/s; deceleration of contact decreases from 43×10^{13} to 8.8×10^{13} cm/s^2; while average density of gold in atmosphere increases from 10.2 to 11.7 g/cm^3. This compaction is a result of cooling: temperature of atmosphere drops from 7.6 to 6.4 kK. Temperature decreases because more cold part of foam are accumulated. Atmosphere becomes thicker mainly due to accretion of foam.

Finishing of subnanosecond interval is shown in figure 12. There are density profiles near contact. Shock in water is far away at the left side; it isn't presented at the spatial scale chosen for figure 12. Shock in water propagates from 870 to 2850 nm during the temporal interval from 250 ps to 1 ns; its velocity decrease from 3 to 2.5 km/s. Compression of water in shock is $\approx 20\%$ at $t = 1$ ns. It seems, that motion of contact weakly influences shock at this stage and later. Thus it decays approximately as $\sqrt{t}$. This is mainly result of stretching of the triangular shock due to dependence of sound speed on pressure (non-linear effect).

Figure 12 demonstrates how the pair from atmosphere and foam evolves. We see that gradually the flux of mass and momentum comes to an end; indeed, at the instant $t = 250$ ps there are a "forest" of fluctuations of density at the right side relative to atmosphere; while at $t = 1$ ns only one fluctuation remains. This is not surprising because amount of mass in foam is limited while the contact always moves more slow than foam—because contact together with atmosphere is dragging by water while foam expands freely. This circumstance ensures finite source of momentum up to exhaustion of foam. We see also that position of the separator "I" in figures 7 and 8 was chosen rightly: there is the last, very slow fluctuation far from atmosphere at the instant $t = 1$ ns in figure 12.

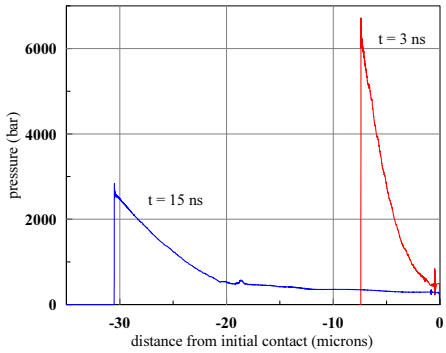

Figure 13. Decrease of pressure in 1D shock in water as it propagates far away from an initiation region in $x = 0$. Formation of pronounced triangular, shock compressed layer behind the shock together with formation of approximately spatially quasi-homogeneous pressure region behind the triangular layer, see profile for $t = 15$ ns.

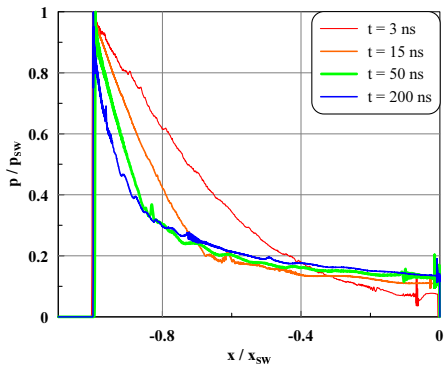

Figure 14. Pressure profiles normalized to the current position and amplitude of the shock in water. This is the late time profiles. They are important for us because they link pressures at the shock and at the contact.

Subsequent decay of the water shock down to subgigapascal amplitudes is shown in figure 13. 1D description of shock propagation is still applicable for usual diameters $2R_L$ of an illuminated spot of the order of hundreds of microns. Transit to 3D propagation will take place when shock runs distance of the order of R_L. Then gradually shape of the shock becomes spherical as in observations [37] and amplitude of the shock begins to decay much faster than the 1D $\sqrt{t}$ law.

For us pressure in water near the contact $p_{\rm CB}$ is significant. It is interesting that $p_{\rm CB}(t)$ is approximately proportional to pressure in the water shock for the time interval after few nanoseconds, see figures 14 and 15. At least this is true until the shock moves in 1D regime.

It is also interesting that after few nanoseconds pressure $p_{\rm CB}(t)$ drops down to saturation pressure $p_{\rm sat}(T)$. After that $p_{\rm CB}(t) = p_{\rm sat}(T_{\rm atm}(t))$, where $T_{\rm atm}(t)$ is defined by cooling of atmosphere from gold; this is the curve "T" in figure 15.

The shifts of contact are of the order of few

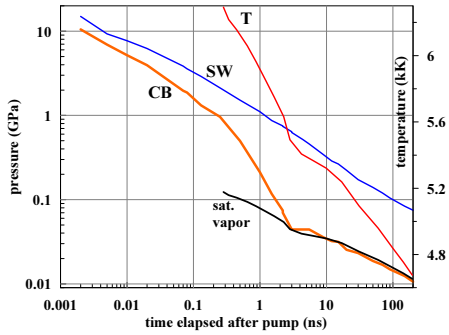

Figure 15. Time dependencies of pressures on shock in water (the curve SW $p_{\rm SW}(t)$) and at the contact boundary (the curve CB $p_{\rm CB}(t)$) between water and gold. Function $p_{\rm SW}(t)$ decays approximately $\propto \sqrt{t}$. While behavior of function $p_{\rm CB}(t)$ is more complicated. It (i) decays slowly while atmosphere was supported by flux of momentum from foam (see figure 9 and 12). (ii) It decays faster at the time interval from subnanosecond to few nanoseconds when the atmosphere becomes unsupported. (iii) From few nanoseconds the function $p_{\rm CB}(t)$ is approximately 10% of pressure $p_{\rm SW}(t)$. The function $p_{\rm CB}(t)$ at this time interval equals to saturation pressure of gold $p_{\rm sat}(T)$ which in turn follows the cooling of atmosphere. The curve "T" gives temperature of atmosphere.

microns thus motion of the contact remains 1D. Although situations with tightly focused laser beam and very small spots $R_L \sim 1$ μm are also possible [38]. Up to now the cases with small spots [38–42] where considered for illumination in vacuum. Analysis of small spots illuminated under water is beyond the scope of this paper.

Dynamic evolution of shock and contact are presented in figure 15. While kinematics of expansion is shown in figures 16-18. Figure 16 gives trajectories of expanding shock and contact. Velocity of propagation of shock changes slowly, thus the curve SW in figure 16 approximately looks like a straight line. Motion of contact passes the same three stages (i), (ii), and (iii) described in the caption to figure 15 for contact pressure. The same three stages are distinctly seen in dependence of velocity $v_{\rm CB}(t)$ in figure 17. Our 2T-HD simulation passes more than 5 orders of time scales from 0.1 ps to 200 ns. Contact velocity drops down $\approx$ 100 times to few tens m/s during this wide time interval and is close to stopping and possible reverse motion.

Contact velocity dependence $v_{\rm CB}(t)$ from figure 17 was analytically approximated by exponential function

$$u_{\rm CB} = 4.0554\ \exp(-0.631255(t_{\rm ps}-1.10875)^{0.23302}). \quad (11)$$

The dependence (11) is presented in figure 17 as the curve "fit". In (11) time $t_{\rm ps}$ is reckoned from maximum of laser pulse in picoseconds [ps], velocity $u_{\rm CB}$ is given in [km/s].

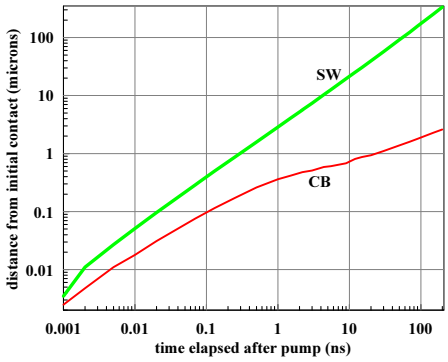

Figure 16. Distances from origin $x = 0$ (initial position of the Au-water contact) passed by a shock (curve SW) and contact boundary (curve CB). In this paper we consider two-temperature hydrodynamic (2T-HD) simulation for absorbed energy 400 mJ/cm^2 and duration of pulse 100 fs.

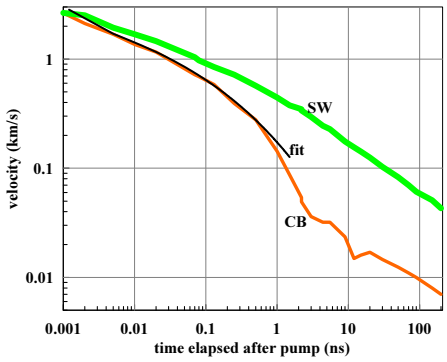

Figure 17. Velocity of contact $v_{\rm CB}(t)$ (curve CB) and velocity of water immediately behind a shock in water (curve SW).

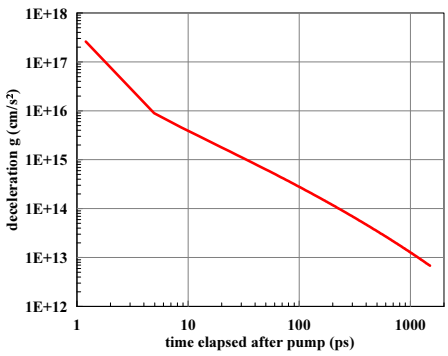

Figure 18. Decrease of deceleration of contact with time. Deceleration is obtained by differentiating of approximation (11). It will be used below for calculations of linear growth of Rayleigh-Taylor instability.

7. Rayleigh-Taylor instability

We study the problem about expansion of gold into surrounding water after ultrashort laser pulse impact through transparent water on absorbing gold surface. In some aspects this problem is similar to the problem called collision of two supersonic counter fluxes [34].

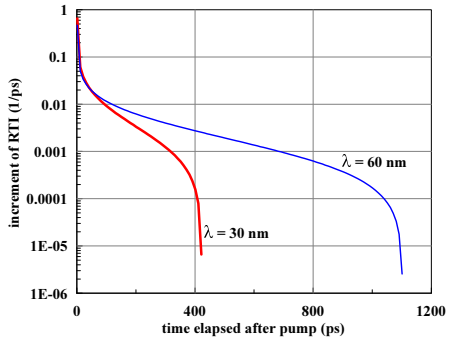

Figure 19. Dependencies of increment (12) on time for the case with $F_{\rm abs} = 400$ mJ/cm^2, $\tau_L = 100$ fs. Finite values of the increment exist at the time interval $0 < t < t_*$, where the instant t_* when growth ends is defined by surface tension. Deceleration is taken from figure 18; $\sigma = 100$ dyn/cm, $\nu = 0.002$ cm^2/s.

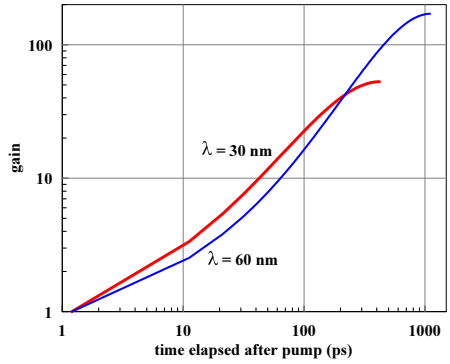

Figure 20. Amplification $a(t)/a(t_0)$ (gain) of perturbation $a(t) = a(t_0)\,\exp(\int^t \gamma(t')\,{\rm d}t')$ for typical wavelengths. We see that there are significant amplifications.

Indeed, we have supersonic shock in water and supersonic flux of two-phase mixture coming from the side of gold. It is known that the contact separating two matters of these two fluxes is often unstable. Rayleigh-Taylor instability may develop [34].

In our case it is obvious that a contact surface is unstable—Rayleigh-Taylor modes may grow. Increment of this instability in the case with surface tension and viscosity [43] is

$$\gamma = \sqrt{(2k^2\nu)^2 + g\,k\,{\rm At} - k^3\sigma/(\rho_A + \rho_w)} - 2k^2\nu. \quad (12)$$

The terms ${\rm At}\,g\,k$, $\sigma\,k^3$., and $\nu\,k^2$ in expression (12) are connected with buoyancy, capillarity, and viscosity, respectively. Density ratio $\rho_A/\rho_w \approx 10$, then Atwood number is ${\rm At}\approx 0.8$. Wavenumber is $k = 2\pi/\lambda$. For waves $\lambda < h$ atmosphere may be regarded as thick because: $k\,h > 2\pi > 1$, here h is height of atmosphere.

To estimate Rayleigh-Taylor growth at a linear stage of development of instability we need data about deceleration $g(t)$ (see figure 18), kinematic viscosity ν of liquid gold (viscosity of water is less significant), and surface tension σ. We take $\nu = 0.002$ cm^2/s from [44]. Surface tension in [dyn/cm] is calculated according to

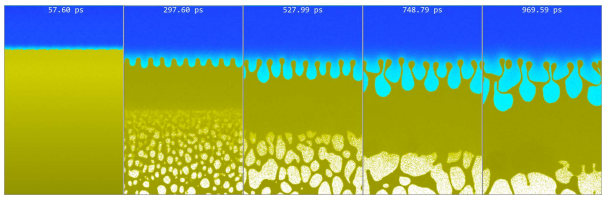

Figure 21. Amplification of Rayleigh-Taylor perturbations as a result of deceleration of dense gold by light water. Gold is yellow, water is blue. Strong heating of water thanks to atom-atom conduction changes color of water from deep blue to light blue. The separated gold droplet is seen in the last frame. This is one of two ways to form nanoparticles; second way is connected with condensation of gold vapor into droplets.

expression [45]

$$\sigma(T) = \sigma_0((1 - T/T_{\rm crit})/(1 - T_m/T_{\rm crit}))^{1.25}. \qquad (13)$$

In (13) $\sigma_0 = 1150$ dyn/cm, $T_{\rm crit} = 7.8$kK is critical temperature, $T_m = 1.338$ kK is melting temperature, From (13) at near critical temperatures we have $\sigma =$ 155, 84, and 25 dyn/cm at $T = 6.5$, 7, and 7.5 kK. Molecular dynamics calculations of coefficient σ is described in [46].

Viscosity damps instability (12) but cannot stop it. Suppression of instability depends on surface tension. Contact becomes unstable if wavelength overcomes capillary scale:

$$k_\sigma = \sqrt{{\rm At}\, g(\rho_A + \rho_w)/\sigma},\ \lambda_\sigma = 21/\sqrt{g_{14}}\,{\rm nm}. \qquad (14)$$

Here we suppose that $\sigma = 100$ dyn/cm, At=0.8, $\rho_A = 10$ g/cm^3, $\rho_w = 1$ g/cm^3, $g = 10^{14}\, g_{14}$ cm/s^2. We see that if we fix surface tension and densities then the capillary scale $\lambda_\sigma(g)$ (14) increases as deceleration $g(t)$ drops down with time. If we fix wavelength λ, then growth of perturbation continues during a finite time interval up to the instant t_*, when deceleration $g(t_*)$ decreases down to the value $g = 10^{14}(21\,[{\rm nm}]/\lambda)^2$. This process is shown in figure 19. Growth of the lager scales λ continues longer but their increment is smaller.

Figure 20 demonstrates how instability develops in linear theory. The parameters are: $\sigma = 100$ dyn/cm, $\nu = 0.002$ cm^2/s, $\rho_A = 10$ g/cm^3, $\rho_w = 1$ g/cm^3; deceleration was defined by expression for velocity (11). From figure 20 we conclude that amplification is rather significant ~ 100 times. Is this enough for transition to non-linear stage? We will use molecular dynamics simulations to answer.

8. Molecular dynamics

Many combined MD-MC molecular dynamics (MD) and Monte-Carlo (MC) runs were carried out to explore the problem with gold expanding to water. MC subroutine describes electron heat conduction in gold. Water in our simulations conducts heat thanks to atom-atom interactions. We vary sizes of simulation box $L_x \times L_y \times L_z$ and initial data (absorbed energy $F_{\rm abs}$). The axis x is directed along expansion. Huge computer resources are necessary for direct MD-MC simulation. Even in simulation up to 3 ns (not 200 ns as in 2T-HD above), thickness of shock compressed water layer is 10 μm, at approximately the same depth

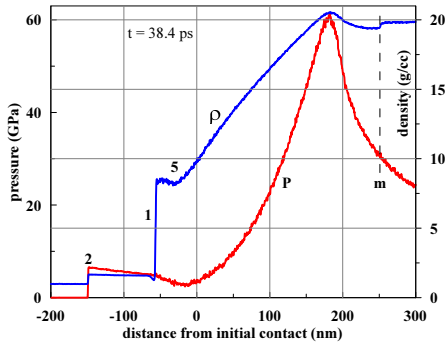

Figure 22. Profiles of p and ρ in MD-MC simulation for narrow channel $L_y = 25$ nm without cut off: full profiles in gold and water. Shock in water is 2, contact is 1, 5 is the boundary of atmosphere. Results are similar to that obtained in 2T-HD simulation.

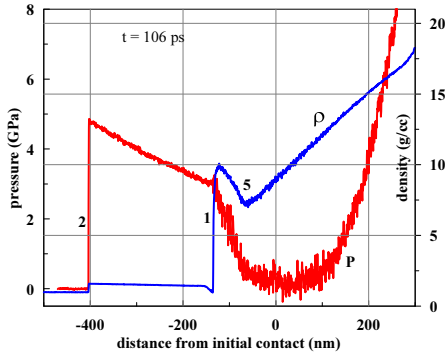

Figure 23. The near contact layer is shown. Compression wave in bulk gold is located at the right side relative to the frame chosen here. Pressure difference at the boundaries of an atmosphere is caused by weight of gold in effective gravity field and by increase of pressure in weak shock separating atmosphere and foam.

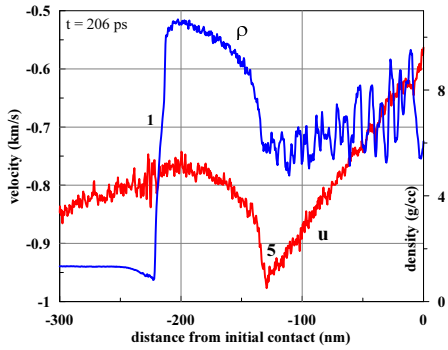

Figure 24. Velocity jump at the upper boundary of an atmosphere where the two-phase vapor-liquid mixture joins atmosphere. Similar pictures are typical for 2T-HD run.

penetrates compression wave in bulk gold during 3 ns. Lateral dimensions should be more than few heights of atmosphere, then $L_y = L_z > 100$ nm. This volume contains more than 10^{10} atoms and simulation is long: few 10^6 time steps.

Therefore we use bypass approach and decrease number of atoms ~ 100 times. First of all we run quasi 3D/2D geometry. Thickness L_z is 8.2 nm (smaller than height of atmosphere). From theory of Rayleigh-Taylor instability we know [34] that quantitatively the 2D and 3D cases differ moderately. Mixing coefficients [34] α_+ are approximately the same. Bubbles rise with similar velocities.

Second, we vary lateral size L_y. We begin simulations with rather narrow size $L_y = 25$ nm to check initial parameters. After that simulation with large size $L_y = 250$ nm has been carried out.

Also we use methods to cut off unnecessary water and gold. Large length $L_{\text{total}} = L_A + L_w$ in x-direction forms due to fast (supersonic) propagation of shock in water and compression wave in gold, see figure 7; here L_A, L_w are distances passed be shocks in gold and water, respectively. While we are interested in much more thin (relative to L_{total}) layer near the contact where velocities are much less than sound speed. Only at acoustic time scale $t_s = d_T/c_s$ contact velocity $u_{\text{CB}}(t)$ is of the order of speed of sound c_s, see figure 17.

Compression wave in gold and near contact layer are separated by foam after finishing of nucleation. Foam is under small pressures and has small speed of sound. Evolution of compression wave in gold doesn't influence dynamics of the near contact layer. Duration of nucleation is of the order of t_s. Nucleation finishes when a rarefaction wave leaves heat affected zone (HAZ) d_T. Therefore at the instant later than duration t_s we can cut off part of foam far from a contact together with bulk gold. This cut off method is used in 2T-HD, see figures 7 and 8. The same method is used in MD-MC runs.

More difficult is situation with water cut off in MD-MC code.

We adjust initial conditions for MD-MC run close to the 2T-HD simulation with $F_{\text{abs}} = 400$ mJ/cm^2, $\tau_L = 100$ fs described above. After that in the run up to 400 ps with small width $L_y = 25$ nm we define trajectory of Lagrangian particle of water $x_{140}(t)$, which before laser action was placed at distance 140 nm from contact. Function $x_{140}(t)$ after the instant $t = 400$ps was analytically continued up to few nanoseconds. To do this we chose a group of water molecules at the distance 140 nm from the initial position of contact. We start simulation and write trajectory of center of mass of this group of molecules. This trajectory gives us the function $x_{140}(t)$. After that in the main MD-MC run we use a water layer limited by the moving boundary $x_{140}(t)$.

Water and gold cut off were combined with 10 times enlarging of width L_y from 25 to 250 nm. Initial stage covering nucleation and first stage of expansion of foam we pass using a narrow channel. After that we multiply ten such channels together obtaining wide channel $L_y = 250$ nm. The width L_y is very important for simulation of development of Rayleigh-Taylor instability.

Results of MD-MC simulation by described above method is presented in figure 21. The upper boundary of the frames shown in figure is defined by trajectory $x_{140}(t)$. Total number of atoms in this particular simulation is near 50×10^6. Thickness of the water layer slowly grows in time because contact pressure decreases, see figure 15. Decrease of pressure decreases density of water. Another effect increasing thickness of the water layer bounded by the wall $x_{140}(t)$ is connected with heating of water near the hot contact.

In figure 21 we see development of perturbations and strong heating of water near contact. It is clear how the process of accretion of foamy two-phase mixture proceeds. There is dense gold vapor inside cells of foam near the contact. Gradually more cold parts of foam arrive to the atmosphere, average temperature of atmosphere decreases, and vapor pressure and concentration decreases. In figure 21 foamy fragments pass weak shock bounding the atmosphere. Cavities collapse passing the shock, pressure and temperature rise, forming continuous media. Atmosphere is a layer of liquid gold bounded by contact with water from one side and by weak shock from the other side.

Pressure in atmosphere increases in direction from weak shock to the contact. Thickness of atmosphere obviously increases with time. This is result of accretion of foam. Thickness increases contrary to gradual cooling and increase of density.

Average profiles obtained in MD-MC simulation from figure 21 for three time instants are shown in figures 22-24. We see that results of MD-MC simulation are close to results of 2T-HD simulation.

9. Conclusion

We have studied action of ultrashort laser pulse onto gold immersed into transparent water. Two codes are used. They are 2T-HD and MD-MC. These codes supplement each other. Indeed, we can follow very long time interval up to 200 ns thanks to 2T-HD code. While MD-MC allows us to see non-trivial non-one-dimensional effects like bombardment of contact with water by fragments of foam. Mechanism of nanoparticles formation connected with hydrodynamic

instability is studied by linear theory and by direct simulation. Those nanoparticles have sizes defined by combined action of surface tension and viscosity.

Acknowledgments

Authors acknowledge support from Russian Science Foundation under prolonged grant 14-19-01599.

References

[1] Kabashin A and Meunier M 2003 *J. Appl. Phys.* **94** 7941–3
[2] Maehara J, Yamada Y, Kumagai H, Midorikawa K and Yabe T 2004 *Jap. J. Appl. Phys.* **43** 172–5
[3] Sylvestre J P, Kabashin A V, Sacher E and Meunier M 2005 *Appl. Phys. A* **80** 753–8
[4] Stratakis E, Barberoglou M, Fotakis C, Viau G, Garcia C and Shafeev G A 2009 *Optics Express* **17** 12650–9
[5] Barcikowski S, Devesa F and Moldenhauer K 2009 *J. Nanopart. Res.* **11** 883–1893
[6] Streubel R, Barcikowski S and Gokce B 2016 *Opt. Lett.* **41** 1486–9
[7] Lescoute E, Hallo L, Hébert D, Chimier B, Etchessahar B, Tikhonchuk V T, Chevalier J M and Combis P 2008 *Phys. Plasmas* **15** 063507
[8] Chimier B and Tikhonchuk V 2009 *Phys. Rev.* B **79** 184107
[9] Itina T 2011 *J. Phys. Chem. C* **115** 5044–8
[10] Povarnitsyn M, Itina T, Levashov P and Khishchenko K 2013 *Phys. Chem. Chem. Phys.* **15** 3108–14
[11] Povarnitsyn M and Itina T 2014 *Appl. Phys. A* **117** 175–8
[12] Shih C Y, Wu C, Shugaev M V and Zhigilei L V 2017 *J. Colloid Interface Sci.* **489** 3–17
[13] Demaske B J, Zhakhovsky V V, Inogamov N A and Oleynik I I 2010 *Phys. Rev.* B **82** 064113
[14] Inogamov N A, Zhakhovskii V V, Ashitkov S I, Petrov Y V, Agranat M B, Anisimov S I, Nishihara K and Fortov V E 2008 *JETP* **107** 1–19
[15] Norman G E, Starikov S V and Stegailov V V 2012 *JETP* **114** 792–800
[16] Anisimov S I, Kapeliovich B L and Perel'man T L 1974 *Sov. Phys. JETP* **39** 375–7
[17] Inogamov N A, Petrov Y V, Zhakhovsky V V, Khokhlov V A, Demaske B J, Ashitkov S I, Khishchenko K V, Migdal K P, Agranat M B, Anisimov S I and Fortov V E 2012 *AIP Conf. Proc.* **1464** 593–608
[18] Povarnitsyn M E, Itina T E, Sentis M, Khishchenko K V and Levashov P R 2007 *Phys. Rev.* B **75** 235414
[19] Petrov Y V, Migdal K P, Inogamov N A and Zhakhovsky V V 2015 *Appl. Phys. B* **119** 401–11
[20] Bushman A V, Fortov V E, Kanel G I and Ni A 1993 *Intense Dynamic Loading of Condensed Matter* (London: Taylor & Francis Translation)
[21] Khishchenko K V, Tkachenko S I, Levashov P R, Lomonosov I V and Vorobev V S 2002 *Int. J. Thermophys.* **23** 1359–67
[22] http://teos.ficp.ac.ru/rusbank/, http://www.ihed.ras.ru/rusbank/ URL `http://teos.ficp.ac.ru/rusbank/` `http://www.ihed.ras.ru/rusbank/`
[23] Petrov Y V, Inogamov N A and Migdal K P 2013 *JETP Lett.* **97** 20–7
[24] Petrov Y V and Inogamov N A 2013 *JETP Letters* **98** 278–84
[25] Petrov Y V, Migdal K P, Inogamov N A and Anisimov S I 2016 *JETP Lett.* **104** 431–9
[26] Migdal K P, Petrov Y V and Inogamov N A 2013 *SPIE Proceedings* **9065** 906503,1–20
[27] Migdal K P, Petrov Y V, Ilnitsky D K, Zhakhovsky V V, Inogamov N A, Khishchenko K V, Knyazev D V and Levashov P R 2016 *Appl. Phys. A* **122** 408[1–5]
[28] Ilnitskiy D K, Khokhlov V A, Zhakhovsky V V, Petrov Y V, Migdal K P and Inogamov N A 2016 *J. Phys: Conf. Ser.* **774** 012101
[29] Hohlfeld J, Wellershoff S S, Guedde J, Conrad U, Jaehnke V and Matthias E 2000 *Chem. Phys.* **251** 237–58
[30] Lin Z, Zhigilei L and Celli V 2008 *Phys. Rev.* B **77** 075133
[31] Ng A 2012 *Intern. J. Quantum Chem.* **112** 150–60
[32] Inogamov N A, Zhakhovskii V V, Ashitkov S I, Khokhlov V A, Petrov Y V, Komarov P S, Agranat M B, Anisimov S I and Nishihara K 2009 *Appl. Surf. Science* **255** 9712–6
[33] Demaske B J, Zhakhovsky V V, Inogamov N A and Oleynik I I 2013 *Phys. Rev.* B **87** 054109 1–9
[34] Inogamov N 1999 *Astrophysics and Space Physics Reviews* **10(Pt.2)** 1–335
[35] Stratakis E, Barberoglou M, Fotakis C, Viau G, Garcia C and Shafeev G 2009 *Optics Express* **17** 12650–9
[36] Inogamov N, Zhakhovsky V, Khokhlov V, Ashitkov S, Emirov Y, Khichshenko K, Faenov A, Pikuz T, Ishino M, Kando M, Hasegawa N, Nishikino M, Komarov P, Demaske B, Agranat M, Anisimov S, Kawachi T and Oleynik I 2014 *J. Phys.: Conf. Ser.* **510** 012041
[37] Tomko J, O'Malley S, Trout C, Naddeo J, Jimenez R, Griepenburg J, Soliman W and Bubb D 2017 **in press**
[38] Inogamov N, Zhakhovsky V, Khokhlov V, Petrov Y and Migdal K 2016 *Nanoscale Res. Lett.* **11** 177(13 pages)
[39] Ivanov D, Rethfeld B, O'Connor G, Glynn T, Volkov A and Zhigilei L 2008 *Appl. Phys. A* **92** 791
[40] Ivanov D S, Lin Z, Rethfeld B, O'Connor G M, Glynn T J and Zhigilei L V 2010 *J. Appl. Phys.* **107** 013519
[41] Ivanov D, Kuznetsov A, Lipp V, Rethfeld B, Chichkov B, Garcia M and Schulz W 2013 *Appl. Phys. A* **111** 675–87
[42] Starikov S and Pisarev V 2015 *J. Appl. Phys.* **117** 135901,1–9
[43] Mikaelian K 1996 *Phys. Rev.* E **54**
[44] Ofte D 1967 *J. Nucl. Materials* **22**
[45] Semenchenko V 1961 *Surface Phenomena in Metals and Alloys* (New York: Pergamon)
[46] Anisimov S, Dunikov D, Zhakhovskii V and Malyshenko S 1999 *J. Chem. Phys.* **110**